Environmental Testing of the NEXT PM1R Ion Engine

IEPC-2007-276

Presented at the 30th International Electric Propulsion Conference, Florence, Italy
September 17-20, 2007

John Steven Snyder,* John R. Anderson*
Jet Propulsion Laboratory, California Institute of Technology, Pasadena, CA, 91109

Jonathan L. Van Noord,† George C. Soulas‡
NASA Glenn Research Center, Cleveland, OH, 44135

The NEXT propulsion system is an advanced ion propulsion system presently under development that is oriented towards robotic exploration of the solar system using solar electric power. The subsystem includes an ion engine, power processing unit, feed system components, and thruster gimbal. The Prototype Model engine PM1 was subjected to qualification-level environmental testing in 2006 to demonstrate compatibility with environments representative of anticipated mission requirements. Although the testing was largely successful, several issues were identified including the fragmentation of potting cement on the discharge and neutralizer cathode heater terminations during vibration which led to abbreviated thermal testing, and generation of particulate contamination from manufacturing processes and engine materials. The engine was reworked to address most of these findings, renamed PM1R, and the environmental test sequence was repeated. Thruster functional testing was performed before and after the vibration and thermal-vacuum tests. Random vibration testing, conducted with the thruster mated to the breadboard gimbal, was executed at 10.0 G_{rms} for two minutes in each of three axes. Thermal-vacuum testing included three thermal cycles from -120 °C to 215 °C with hot engine re-starts. Thruster performance was nominal throughout the test program, with minor variations in a few engine operating parameters likely caused by facility effects. There were no significant changes in engine performance as characterized by engine operating parameters, ion optics performance measurements, and beam current density measurements, indicating no significant changes to the hardware as a result of the environmental testing. The NEXT PM1R engine and the breadboard gimbal were found to be well-designed against environmental requirements based on the results reported herein. The redesigned cathode heater terminations successfully survived the vibration environments. Based on the results of this test program and confidence in the engineering solutions available for the remaining findings of the first test program, specifically the particulate contamination, the hardware environmental qualification program can proceed with confidence.

I. Introduction

NEXT (NASA's Evolutionary Xenon Thruster) is an advanced ion propulsion system developed by a team led by the NASA Glenn Research Center (GRC) that is oriented towards robotic exploration of the solar system using solar electric power.[1] Potential mission destinations that could benefit from a NEXT solar electric propulsion system include inner planets, small bodies, and outer planets and their moons.[2] This range of robotic exploration missions generally calls for ion propulsion systems with deep throttling capability and system input power ranging

* Senior Engineer, Advanced Propulsion Technology Group.
† Aerospace Engineer, Propulsion and Propellants Branch, 21000 Brookpark Road, Cleveland, OH 44135, MS 16-1.
‡ Electrical Engineer, Propulsion and Propellants Branch, 21000 Brookpark Road, Cleveland, OH 44135, MS 16-1.

from 5 to 25 kW, as referenced to solar array output at 1 Astronomical Unit (AU). In order to ensure that the NEXT system can successfully perform these missions, its components will be subjected to qualification-level testing that is representative of the anticipated environments.

The NEXT ion propulsion subsystem development includes a 7-kW high efficiency ion thruster, modular power processing unit (PPU), advanced propellant management system (PMS), lightweight gimbal, and software algorithms for a digital control interface unit (DCIU). Individual components in a subsystem such as this are typically subjected to separate environmental test sequences, partially due to the different environments each will experience on a spacecraft. For the test program discussed in this paper, the thruster and gimbal were tested together as an assembly in vibration environments. The thruster was tested alone in thermal environments.

The NEXT ion thruster is a 7-kW, 36-cm-beam-diameter thruster with significant heritage to the 2.3-kW, 30-cm NSTAR engine which flew on the Deep Space 1 mission[3] and is an integral part of the Dawn spacecraft scheduled for launch in late 2007.[4] Initial thruster development work was led by GRC and included significant performance testing,[5] a 2000-hour wear test,[6] an integrated test with other subsystem components,[7] and more recently an ongoing wear test[8] and a multi-thruster array test.[9] The thruster technology was transferred to NEXT industry partner Aerojet, which designed and fabricated a flight-like Prototype Model (PM) thruster.[10] Following performance acceptance testing at GRC,[11] the PM1 ion engine was sent to JPL for extensive environmental testing. First the engine was subjected to a thermal balance test[12] in which the engine, instrumented with tens of thermocouples, was tested under a variety of operating conditions and thermal environments to characterize engine temperatures and thermal design margins. Data from that test were used in developing and validating an engine thermal model.[13]

Following the thermal balance test the PM1 engine was subjected to an environmental test program[14] in the latter half of 2006. Although the testing was largely successful there were several findings. The major issues encountered during the vibration test sequence were discharge and neutralizer heater impedance variations, particulate contamination generation, and fastener backouts on both the thruster and gimbal. Significant particulate contamination inside the engine was observed and was traced to fragmentation of the potting cement on the cathode heater terminations, nutplate wear, residue remaining inside the engine from manufacturing processes, and fraying fiberglass wire insulation. In many instances the amount of contamination generated was in excess of typical spacecraft cleanliness requirements. Additionally, during the third and final thermal cycle of the thermal-vacuum testing the neutralizer heater failed to pass current, most likely related to the impedance anomalies observed in vibration testing. Despite these findings, the thruster performance was nominal throughout the test program. There were noticeable changes in some thruster operational parameters, likely related to modest differences in tank pressure between different test phases, but no indication of a major change in thruster performance or operation resulting from exposure to the vibration and thermal environments. Similarly, there was no major change in ion optics performance or beam current density data. Although neutralizer cathode ignition times were consistent and showed little dependence on temperature, the discharge cathode ignition times showed a strong dependence on temperature.

Most of the findings of the PM1 environmental test program were addressed during engine re-design activities performed at Aerojet, GRC, and JPL in late 2006 and early 2007.[15] The most significant work was focused on structural re-design of the cathode heater electrical terminations. Fastener loosening, electron backstreaming, nut plate galling, and fraying fiberglass wire insulation were also addressed. Complete resolution of all contamination issues was not possible with the reworked hardware, specifically the particulate contamination due to manufacturing processes, but engineering solutions are available and validation is planned with subsequent hardware builds. The re-worked engine, renamed PM1R, was successfully subjected to performance acceptance testing at GRC in mid-2007 and subsequently shipped to JPL for the repeated environmental testing which is reported here.

The NEXT gimbal development was led by JPL. The breadboard gimbal is a lightweight, two-axis design using a four-bar linkage mechanism that provides a positive captured configuration for launch while providing for up to twenty degrees of thrust angle articulation while in the operational configuration.[16] JPL contracted with Swales Aerospace for the design and fabrication of two breadboard gimbals. The primarily-aluminum gimbal structure resembles an A-frame with titanium used for the flexures and the thruster mounts. An additional supporting bracket is required to support the mass of the gimbal motor. In addition to the first thruster-gimbal vibration test, the breadboard gimbal was successfully subjected to vibration testing with a thruster mass model in an earlier test.[17]

The objectives of the environmental test program were as follows:

- To validate the NEXT PM1R thruster and breadboard gimbal assembly to qualification-level dynamic environments, including:
    - Demonstrate thruster functionality pre- and post-vibe
    - Demonstrate gimbal functionality pre- and post-vibe

- To validate the NEXT PM1R thruster to expected mission thermal environments, including standard qualification margins, including:
    - Expose the thruster to expected mission temperatures in cycles
    - Demonstrate thruster functionality pre- and post-test

Environmental test requirements for the thruster and gimbal were determined from the NEXT project requirements, expected mission environments, and JPL assembly-level environmental verification policies and requirements. Discussion of the test requirements may be found in Section II, along with test equipment and facility setup information, and test methods. Test results are presented in Section III.

II. Test Setup and Methods

A. Test Article and Equipment

1. Thruster and Gimbal

The thruster used for the environmental testing described herein was the re-worked NEXT Prototype Model 1 (PM1R) thruster. The thruster was originally manufactured and subsequently re-worked by Aerojet (Redmond, WA) under direction of the NASA Glenn Research Center. Significant changes in the PM thruster design compared to the previous generation of thruster designs include new material coatings to increase emissivity for enhanced thermal margin, more uniform ion optics apertures, and a graphite discharge cathode keeper to mitigate keeper erosion. Additional information about the PM1 engine, including performance data, is presented in Ref. 11. Brief descriptions of the modifications for the PM1R engine are discussed in Ref. 15. The cathode heater terminations were modified to be similar to the flight-proven Space Station Plasma Contactor design. Electron backstreaming was addressed through reducing the open-area fraction of the plasma screen. Fiberglass sleeving used for wire insulation was removed from the accessible internal wiring, but not at the main harness pass-through on the plasma screen. Loosened fasteners and nut plate galling were corrected with updated torque values and fastener types.

Breadboard gimbal S/N 001 was used as the test article for the functional and vibration testing described herein. The breadboard gimbal was designed and fabricated to be flight-like, e.g. all fabricated parts were of JPL-approved materials with certifications. The motors chosen for the NEXT breadboard gimbal were ultra-high-vacuum class stepper motors. A flight unit would use space-rated versions with complete Quality Assurance documentation. The only functional difference between the two motor grades is the lower minimum temperature of the space-grade motor. The flight configuration of the gimbal has pinpullers specified as a launch lock for the actuator arm. This feature was not required for the breadboard gimbal, so a fixed-pin bracket was fabricated to replicate the launch lock function. All non-locking fasteners were locked or staked with Solithane, a flight-grade thread locking agent. All gimbal parts were demonstrated by analysis to meet allowable stress levels and minimum frequencies based on the predicted flight loads. Gimbal S/N 001 was vibrated under identical random vibration loads as to be used for the testing described herein with the PM1 thruster[14] and a thruster mass model.[17]

2. Vacuum Test Facility

The thruster test portions of the PM1R environmental test program were conducted in the JPL Patio Chamber facility. The vacuum chamber is 3 m in diameter and 8.6 m long, with ten cyropumps installed and operational for this testing. With the vacuum chamber configuration used for this test, specifically the inclusion of the large engine thermal shroud, the effective pumping speed was approximately 200,000 L/s on xenon. To minimize facility backsputter rates the interior of the vacuum facility is lined with graphite panels, which tended to absorb atmosphere gases and water vapor during the vacuum cycles of the testing. Modest tank pressure variations were observed as the panels outgassed during thruster operation. To mitigate this effect, a full-power thrusting operating phase was added prior to functional testing to bake out the panels.

The thruster was installed in a 1.2-m diameter by 1.0-m long cylindrical thermal shroud located at one end of the vacuum facility. The downstream end of the thermal shroud was located 6.2 m from the downstream end of the vacuum facility. The thruster was mounted inside the shroud with the neutralizer keeper orifice plate located 5.7 cm from the downstream end of the shroud. The cylindrical and rear thermal shroud walls were equipped with liquid nitrogen tubing to provide environmental cooling of the test article. The opening at the front of the shroud was equipped with a door made of multi-layer insulation. This door was opened during thruster operation and could be closed to minimize thermal interaction with the vacuum facility during non-operational cold soak periods.

The thermal shroud was also equipped with eight quartz infrared heat lamps to provide environmental heating to the thruster. The lamps were installed parallel to the thruster axis and spaced 45 degrees apart azimuthally with one end of the lamp even with the front mask of PM1R. A temperature controller and SCR power controller were used for tight process control during temperature ramp and hold. A photograph of the test setup with the heat lamps operating is shown in Fig. 1. In contrast to the Thermal Development Test[12] where the heat lamps were controlled through the heat flux coupons mounted near the engine, in the thermal vacuum test the heat lamps were directly controlled through the temperature of gimbal pad A. Gimbal pad A was located at the 6 o'clock position as viewed in Fig. 1 (i.e. opposite the neutralizer); pads B and C were located at the 10 o'clock and 2 o'clock positions, respectively. Gimbal pad A was chosen as the reference location because it was the coolest of the three gimbal pads during preliminary testing.

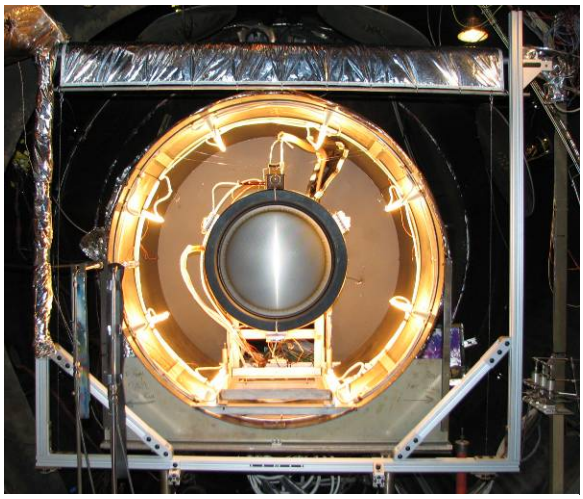

Fig. 1. Test Setup for Functional and Thermal Vacuum Testing.

The thermal shroud and facility were equipped with more than twenty thermocouples for process control and monitoring. The thruster propellant lines internal to the thermal shroud were wrapped with heater tape, instrumented with thermocouples, and wrapped in an MLI blanket to control the temperature of the lines during thruster cold soaks and periods prior to engine startup.

Beam current density profiles were measured with two Faraday probes. The probes were installed on a stage that allowed them to translate through the thruster plume at axial distances between 0.045 m and 0.55 m downstream of the thruster.

The environmental testing was performed using laboratory power supplies controlled and monitored by a data acquisition and control system. Dedicated cathode ignitor circuits were used for cathode ignition and grid recycling was handled by a custom recycle circuit. Flow and electrical instrumentation were calibrated prior to the testing. The data acquisition system recorded thruster currents, voltages, flow rates and temperatures, and facility pressure and temperatures at a user-specified rate. Data were typically recorded once a minute; however, during thruster starts or when thruster parameters were being varied the rate was often changed to once every ten seconds. The software used to record data was also used to control thruster power supplies and flow rates. Closed-loop control of flow rates and beam current was used, the latter by adjusting discharge current.

3. Vibration Test Setup and Facility

The thruster was mated to the breadboard gimbal for vibration testing, as shown in the test setup photograph of Fig. 2. The thruster-gimbal assembly was mounted on a vibration fixture, comprised of a vibration test plate and three vibration test mounts, which provided the mechanical interface between the vibration table and the test article. The engine was fixed to the gimbal at each of the three gimbal legs. Each gimbal leg rested on a vibration test mount, and four piezoelectric three-axis force transducers were mounted between each test mount and the vibration test plate. These were used for vibration force limiting, discussed later. Gimbal legs were annotated the same as the thruster pads, i.e. leg A was located opposite the neutralizer.

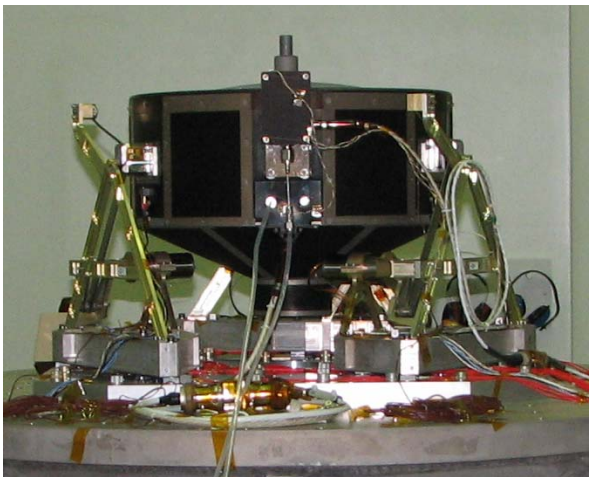

Fig. 2. Test Setup for Z-Axis Vibration.

The test assembly was instrumented with a total of seventeen tri-axial and one uni-axial response accelerometers. All accelerometers were bonded to Kapton tape applied to the test article surfaces. Nine tri-axials were mounted on the vibration test mounts near the gimbal strut attachment points. Three tri-axials were located on the side of the gimbal brackets that mount to the thruster, and three other tri-axials were mounted on the

thruster directly below the interface with the gimbal bracket. The remaining two tri-axials were mounted on the neutralizer and the neutralizer support pad, and the lone uni-axial accelerometer was mounted on the unperforated region of the accelerator grid directly opposite the neutralizer.

Vibration testing was performed in the JPL Dynamics Environmental Test Facility. Vertical (i.e. Z-axis, or thrust axis) excitation was performed on a Kimball head expander on the large spacecraft vibration test stand. Lateral (X- and Y-axis) excitation was performed on a separate oil-lubricated slide plate. Application of vibration to the test article was controlled using one of JPL's m+p vibration control systems. Vibration test control instrumentation consisted of two control accelerometers and one monitor accelerometer mounted to the vibration test plate. This was in conjunction with the signal from the twelve force transducers at the unit interface, controlling all random vibration tests using the extremal control mode. Data acquisition from control and response accelerometers was provided at a 20 kHz sampling rate.

B. Test Methods

The environmental test program was performed in the sequence of steps shown in Table 1. Additionally, hardware inspection was performed prior to the first and after each of the test segments. This included visual inspection, electrical diagnostics, and in some cases disassembly of test hardware. Notable inspection results are described in the appropriate sections of this paper. Thruster and thruster/gimbal functional testing was performed prior to and after each test segment to demonstrate operation over requirements after exposure to environments.

1. Thruster Functional Test

Thruster functional testing was performed prior to the vibration testing to demonstrate nominal engine operation, including: engine performance, neutralizer characterization, electron backstreaming and perveance margins, double-to-single ion current ratios, and beam current density profile. Thruster functional testing was repeated after vibration testing and thermal-vacuum testing.

Table 1. Environmental Test Sequence.

Sequence	Operation
1	Pre-Vibe Thruster Functional Test
2	Pre-Vibe Gimbal Functional Test
3	Random Vibration Tests
4	Post-Vibe Gimbal Functional Test
5	Post-Vibe Thruster Functional Test
6	Thermal Vacuum Test
7	Post-Thermal Thruster Functional Test

Testing of the NEXT PM1R thruster was conducted using laboratory power supplies and a laboratory flow system. A total of four Functional Test Points (FTP) were used during the environmental testing; the thruster controlled parameters are listed in Table 2 for those conditions as well as the startup conditions (i.e. Discharge-Only). Seven parameters were specified for a given operating condition: the propellant flow rates to the discharge chamber, cathode, and neutralizer; the extraction parameters beam current, beam voltage, and accelerator grid voltage; and the neutralizer keeper current. Note that in practice it was the screen power supply voltage that was controlled and the beam voltage was calculated from the sum of the power supply voltage and the neutralizer floating voltage. Beam current was controlled by adjusting the discharge current, often performed automatically with closed-loop control through the data acquisition and control system. Operating conditions are referenced in this report by the combination of beam current and voltage.

Thruster operating parameters were continuously recorded by the data acquisition system during the thruster functional performance testing. In addition to the controlled parameters, the following parameters were recorded: accelerator grid current, discharge current and voltage, cathode keeper voltage, neutralizer keeper voltage, neutralizer-common-to-ground voltage, and tank pressure. Common calculated or derived parameters were also determined: thrust, specific impulse, total efficiency, and beam ion energy cost (also called discharge losses). Floating (i.e. neutralizer coupling) voltages were in the range of -9.9 to -11.7 V for this testing.

Table 2. Thruster Controlled Parameters for Functional Testing.

Control Parameter	Discharge-Only	FTP 1	FTP 2	FTP 3	FTP 4
Beam Current (A)	-	1.20	2.00	3.52	3.52
Beam Voltage (V)	-	679	1179	1179	1800
Accelerator Voltage (V)	-	-115	-200	-200	-210
Neutralizer Keeper Current (A)	3.0	3.0	3.0	3.0	3.0
Main Flow Rate (sccm)	14.23	14.23	25.79	49.64	49.64
Cathode Flow Rate (sccm)	3.57	3.57	3.87	4.87	4.87
Neutralizer Flow Rate (sccm)	6.00	3.00	2.50	4.01	4.01

Ion optics performance was measured using standard procedures. Perveance measurements were made by holding the beam current and accelerator grid voltage constant while varying the screen grid voltage and recording the accelerator grid current. The discharge current was adjusted in this case to maintain constant beam current. The perveance limit was defined as the total voltage at which the rate-of-change of accelerator grid current was -0.02 mA/V. Electron backstreaming (EBS) onset was determined by reducing the magnitude of the accelerator grid voltage at constant discharge current and monitoring the beam current. A 1-mA increase in the beam current from the lowest current achieved during the measurement defined the EBS limit. In practice, the voltage drop across the calibrated beam current shunt resistor was used to determine this limit.

Neutralizer characterization was performed in the discharge-only mode conditions shown in Table 2 by decreasing the neutralizer flow rate until the neutralizer transitioned from spot to plume mode. Plume mode, characterized by electrical oscillations in the neutralizer keeper circuit, was defined as reaching or exceeding 5 V peak-to-peak oscillations measured between neutralizer keeper and neutralizer common.

2. Gimbal Functional Test

Gimbal functional testing was performed with the thruster integrated onto the gimbal and the assembly mounted to the vibration test fixturing. Since the gimbal is a zero-G design that cannot adequately support and drive the thruster mass in a one-G environment, the thruster-gimbal assembly was fitted with a system of weights and pulleys for functional testing to offload the thruster mass. Offloading was applied equally at each gimbal pad through a fastener attached to each gimbal thruster bracket as shown in Fig. 3. The gimbal was driven via a custom software program and dedicated motor control hardware.

Functional testing was accomplished by driving the gimbal to a range of nineteen positions which described and circumscribed the range of motion. At several of the sequence steps, an inclinometer was used to measure the gimbal pitch in two orthogonal axes. Accuracy of the inclinometer measurement was estimated to be ±0.5° and all measurements were rounded to the nearest degree. After returning to the stowed position, the pin-puller mockups were re-inserted into the assembly and their fit used to determine if the stepper motors returned to the correct final position (i.e. there were no missed steps during the functional test).

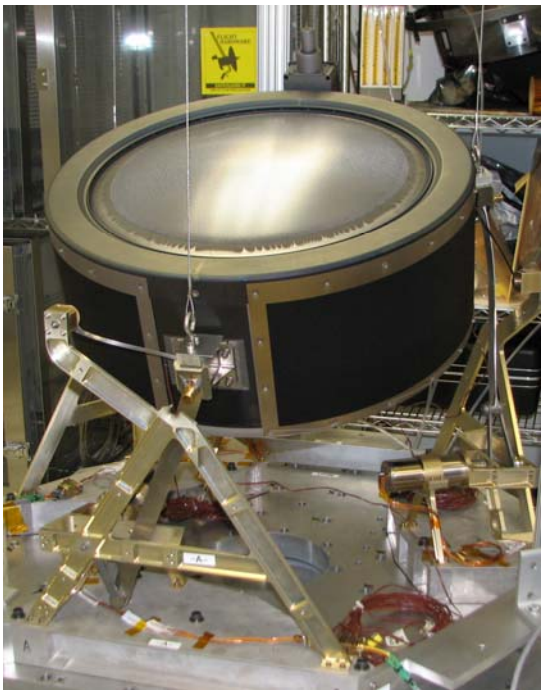

Fig. 3. Gimbal Functional Test.

3. Vibration Test

The random vibration specification for the NEXT thruster-gimbal assembly was based on Delta-class launch vehicles and typical locations of electric propulsion hardware on spacecraft. The qualification-level specification, shown in Table 3, has a total level of 10.0 G_{rms} and calls for random vibration testing in each of three orthogonal axes for a duration of two minutes per axis. Sine surveys were performed before and after each full-level random vibration test to identify hardware changes caused by testing. The surveys were run at a load of 0.25 $G_{0\text{-}pk}$ from 5 to 2000 Hz at a sweep rate of two octaves per minute.

Table 3. Qualification-Level Random Vibration Requirements.

Frequency (Hz)	Level
20 Hz	0.04 g^2/Hz
20 – 50 Hz	+3 dB/octave
50-600 Hz	0.1 g^2/Hz
600 – 2,000 Hz	-6 dB/Octave
2000 Hz	0.009 g^2/Hz
Overall	10.0 G_{rms}

Duration: 2 min./axis, 3 orthogonal axes

Vibration testing of the NEXT thruster-gimbal assembly also incorporated the practice of force-limited vibration testing which is used for most vibration tests performed at JPL. Force-limiting during vibration testing guards against artificial test failures caused by overtesting, a result of the infinite mechanical impedance of the shaker and the use of only acceleration-based control.[18] In this situation, the reaction forces at the fixture/engine interface can become unrealistically high compared to a flight environment at test article resonances. In a force-limited test, real-time force measurement and limiting is performed to notch the input acceleration spectrum.

Vibration testing in the Z-axis (i.e. thrust axis) was performed first, followed by the lateral axes Y (i.e. axis intersecting both the discharge chamber and neutralizer centerlines) and finally X. After the Z-axis testing was completed the test assembly including vibration fixturing was removed from the head expander and was attached to the slip plate for lateral axis testing. For all axes, the first activity was a sine survey of the assembly. This was followed by a random vibration test at a level of -18 dB with respect to the full random vibration loads shown in Table 3 in order to verify instrumentation operation and tune the vibration force-limiting algorithms. The full-level random vibration test was then performed, followed by a final sine survey. Physical inspections of the test assembly were performed after each of these tests.

4. Thermal Vacuum Test

Requirements for the thermal vacuum test were derived from mission studies and simple spacecraft configuration models. The NEXT system design has been driven by Deep Space Design Reference Missions as well as by Discovery and New Frontiers class missions.[19] Preliminary modeling of the NEXT PM-design thruster on a sample spacecraft configuration showed that the most aggressive thermal conditions were projected to occur during Venus gravity assists on trajectories to Saturn and Neptune, specifically at 0.85 A.U. and with a solar incidence angle of 38º from the thruster exit plane.[10] A more rigorous thermal model of the NEXT thruster was recently developed in conjunction with the PM1 Thermal Development Test[12] and validated with data from that test.[13]

A departure from standard practice was made with the selection of reference temperature location on the NEXT engine. On the Deep Space 1 mission, a location on the front mask of the NSTAR ion engine was used as the reference temperature location for environmental testing and flight telemetry.[20] It was very difficult, however, to correlate the reference location temperature with the internal thruster temperatures because the mask was not well coupled to the engine through thermal conduction and knowledge of the surface optical properties was poor. Evaluation of data from the PM1 Thermal Development Test combined with the thermal model of the engine suggested that the engine gimbal pads would be a more appropriate location for temperature reference.

The NEXT PM1R thermal model, updated to reflect pertinent design changes, was employed in a simple spacecraft configuration model at the projected mission worst-case solar irradiance to determine maximum expected gimbal pad temperatures in this environment. With the reduced open-area fraction of the plasma screen mesh compared to PM1, the maximum expected temperature increased from 187 °C (see Ref. 13) to 195 °C. The thermal-vacuum test maximum temperature for PM1R was thus 215 °C including the standard flight temperature margin. The cold temperature limit for NEXT thermal-vacuum testing was not derived from corresponding mission analyses and thermal modeling; ion thrusters can survive much lower temperatures than the -100 °C levels typically required for flight systems. For the testing described herein, a cold temperature of -120 °C was chosen which was 11 °C colder than the Deep Space 1 qualification requirement for the NSTAR ion engine. [20]

The plan for the thermal vacuum test called for three identical thermal cycles. The cycles consisted of:

1. Two-hour minimum cold soak after reaching the cold temperature limit of -120 °C.
2. Short-duration operation in discharge-only mode at full-power conditions.
3. Full-power operation ramp to the hot temperature limit of 215 °C.
4. Four hours of operation at full power (3.52 A and 1800 V).
5. Four hours of operation at mid power (3.52 A and 1179 V).
6. Turn off engine, then immediately begin cathode ignition sequence.
7. Short-duration operation in discharge-only mode, then at full power conditions.
8. Turn off engine and cool for next cycle.

A schematic of the test profile is shown in Fig. 4. In this test profile, three cold starts and three hot starts were included. The planned total cumulative cold soak time was 6 hours and total cumulative hot operation time was 24.5 hours. All discharge-only operation during thermal-vacuum testing was performed at discharge conditions equivalent to full power operation (i.e. 3.52 A and 1800 V). Engine operating parameters were recorded continually throughout the test as described in Section II. After approximately three hours of operation at each of the two beam extraction operating points, electron backstreaming and beam current density data were acquired.

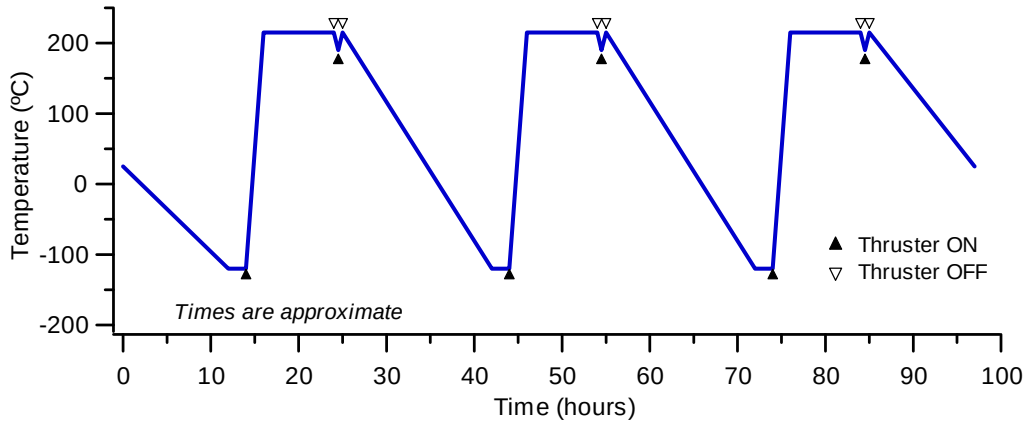

Fig. 4. Thermal Vacuum Test Plan Temperature Profile.

III. Test Results

A. Pre-Vibration Thruster Functional Test

Thruster functional testing was performed at the beginning of the environmental test program to establish a baseline against which post-environmental performance could be compared. Non-controlled and derived engine performance parameters for the highest power and a mid power operating condition are compared in Table 4 for the PM1[14] and reworked PM1R pre-vibration functional tests. Note, as will be seen in the data presented in a subsequent section of this paper, the differences between the PM1 and PM1R data are not significantly different from the scatter typically seen between different tests with the same engine. The modest differences in the discharge parameters and accelerator grid current are likely due to differences in the tank pressures, which were higher by about 10% in the PM1 testing. Note that at higher background pressures there is more mass ingestion into the discharge chamber, and standard operating procedure for the NEXT test program is not to correct the main flow into the thruster for ingestion, which can affect the calculated beam ion energy cost and total thruster power through the measured discharge power. Apart from these noted parameters, there was no significant difference observed in the engine performance data. Ion optics performance margins were also comparable, within the typical measurement error and data scatter. As expected, the rework done on the thruster had no apparent effect on the measured engine performance.

Table 4. Comparison of Pre-Vibration Engine Performance Data for PM1[14] and PM1R Thrusters.

	3.52 A, 1800 V		2.0 A, 1179 V	
	PM1R	**PM1**	**PM1R**	**PM1**
Discharge Current (A)	18.6	18.1	14.2	13.9
Discharge Voltage (V)	24.4	23.2	24.2	24.5
Cathode Keeper Voltage (V)	5.5	5.4	3.6	3.9
Accelerator Grid Current (mA)	25.9	20.8	10.8	7.2
Neutralizer Keeper Voltage (V)	11.8	12.0	13.5	13.3
Power (W)	6890	6860	2750	2760
Thrust (mN)	237	238	108	109
Specific Impulse (sec)	4180	4190	3470	3500
Total Efficiency	0.705	0.712	0.668	0.677
Perveance Margin (V)	1150	1156	708	686
Electron Backstreaming Margin (V)	43	49	101	101

B. Pre-Vibration Gimbal Functional Test

Starting from the stowed position, the gimbal was first driven to the 'clear latch' position to ensure that the thruster pins cleared the gimbal A-frames acceptably. The gimbal was then driven to each of the positions shown in Table 5 and the inclination was measured at gimbal thruster bracket A (i.e. the gimbal bracket attached to the thruster, located opposite the neutralizer) in the radial and tangential directions. The total range of the gimbal at this bracket was measured as -19°/+20° in the radial direction and +16°/-17° in the tangential direction. The full nineteen-step drive program was then successfully performed to exercise the gimbal motion with the attached thruster. Following completion of the sequence, the pin-puller mockups were re-inserted into the gimbal demonstrating successful and complete return to the stowed and latched position.

Table 5. Pre-Vibe Gimbal Articulation Measurement Results.

Position Name	Gimbal Pad A Elevation (cm)	Radial Inclination	Tangential Inclination
Stowed, Latched	0	0°	0°
Clear Latch	2	0°	0°
Mid Plane	10	0°	0°
Max A, Level B, Level C	17	-8°	0°
Max A, Min B,C	17	-19°	0°
Min A, Max B,C	1	20°	0°
Mid Plane	10	0°	0°
Level A, Min B, Max C	10	0°	16°
Level A, Max B, Min C	10	-0°	-17°
Stowed, Latched	0	0°	0°

C. Thruster-Gimbal Assembly Vibration Test

1. Z-Axis Testing

Dynamic testing began with the Z-axis (i.e. thrust-axis) testing, shown in the photograph of Fig. 2. Initial tests and then the two-minute full random vibration test were completed without incident. The vibration test inputs, which were notched automatically and in real time during the test according to the force limit specifications, are shown in Fig. 5. Significant notches were observed at 100, 760, and 1130 Hz, similar to the behavior of the previous test.[14]

Comparison of the pre- and post-vibe sine surveys showed significant changes on all in-axis accelerometers on the thruster and gimbal near the fundamental mode. A typical response is shown Fig. 6 for the accelerometer mounted on thruster gimbal pad B, just underneath the gimbal bracket. A frequency shift of roughly 10% was observed near 100 Hz with little-to-no evidence of a change in response damping, for all accelerometers on the thruster and gimbal and for the measured in-axis force sum. The frequency shift is larger than what is nominally observed in run-to-run comparisons and merits additional investigation.

In contrast to the changes observed on the thruster and gimbal, there was little change observed in the data from accelerometers located on the vibration test mounts, as shown in the representative data of Fig. 7. These results collectively indicate that changes occurred in the test article and not at the structural bolting interface between the vibration fixturing and the vibe table.

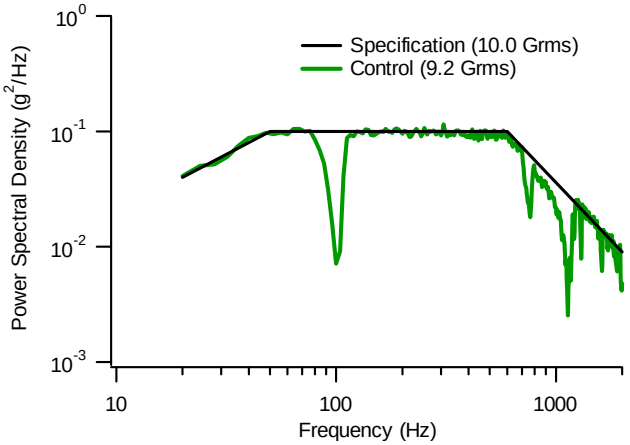

Fig. 5. Comparison of Random Vibration Specification with Force-Limited Test Inputs, Z-Axis Excitation.

Inspection of the test assembly immediately after the Z-axis testing did not reveal any clear causes for the sine survey shifts observed in the data. Frequency shifting and some damping have been observed in previous Z-axis testing with this gimbal[14,17] and it is believed that these shifts are due to settling in the hardware at the capture interface between the thruster pin and the gimbal frame but this has not yet been proven. At present, additional analyses are underway to understand this issue and determine if any design changes are necessary. Nevertheless, as will be shown, there was no observed effect on the ability of the gimbal or thruster to pass post-vibe functional tests.

2. Lateral Axis Testing

Dynamic testing continued with the Y-axis testing, which was completed without incident. Following the Y-axis testing the test assembly was rotated 90° to perform the X-axis random vibration testing, shown in the test setup of Fig. 8. The X-axis test sequence including the two-minute full random vibration test was also completed without incident. The vibration test inputs for both X and Y excitation are shown in Fig. 9. Significant notches in the control acceleration spectrum were observed at 76 and 400 Hz for the Y-axis excitation, and at 80 and 380 Hz for X-axis excitation.

Comparison of the Y-axis pre- and post-vibe sine surveys showed only minor changes in the test assembly near the fundamental mode in the frequency range of 50-100 Hz. Larger differences were seen in the X-axis comparisons; typical data are shown in Fig. 10, similar differences were observed throughout the other accelerometers on the test article. A sizable narrow-band peak near

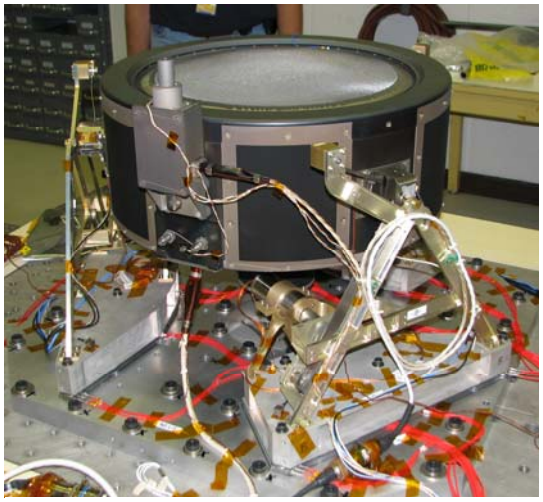

Fig. 8. Test Setup for X-Axis Vibration.

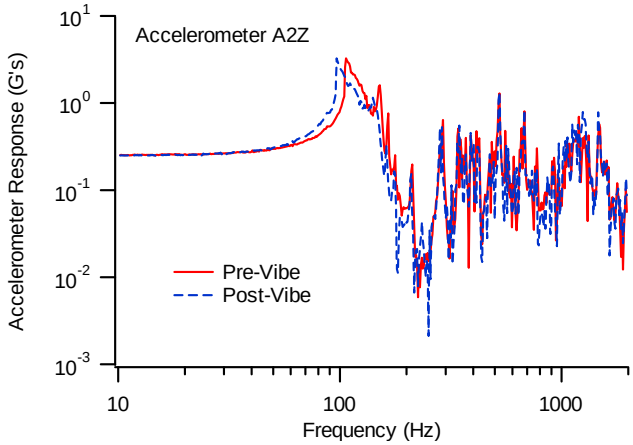

Fig. 6. Comparison of Sine Survey Results Before and After Full-Level Z-Axis Random Vibration, Thruster Gimbal Pad B.

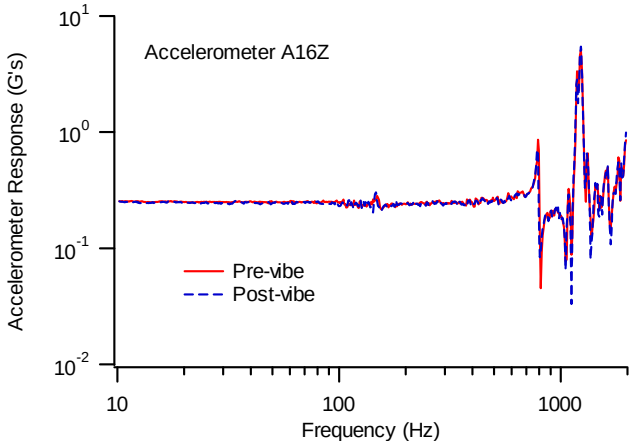

Fig. 7. Comparison of Sine Survey Results Before and After Full-Level Z-Axis Random Vibration, Vibe Test Mount C, Near Free Leg.

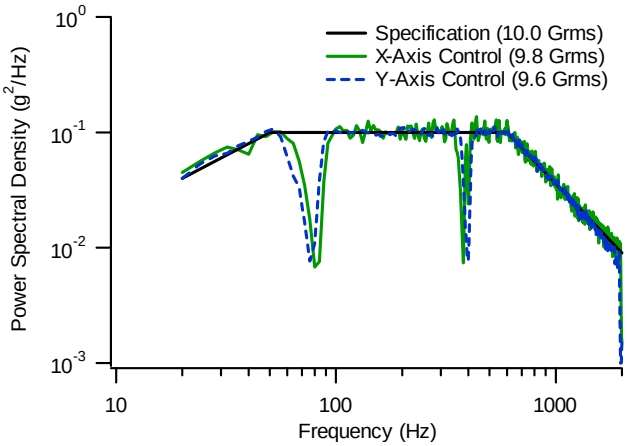

Fig. 9. Comparison of Random Vibration Specification with Force-Limited Test Inputs, Lateral Axis Excitation.

the fundamental mode that was observed before the full random vibration test did not appear afterward. This peak was also observed in the PM1 vibration test of 2006, but did not decrease as seen in Fig. 10. As for the Z-axis results, the accelerometers on the vibration test mounts did not show any significant difference for either Y-axis or X-axis testing. This result is an indication that changes occurred in the test article and not at the structural bolting interface between the vibration fixturing and the vibe table. As noted earlier, these sine survey changes are presently under investigation.

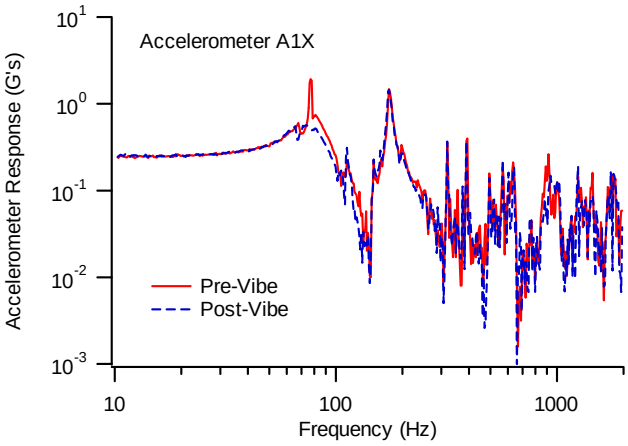

Fig. 10. Comparison of Sine Survey Results Before and After Full-Level X-Axis Random Vibration, Thruster Gimbal Pad A.

3. Post-Vibration Inspection Results

The thruster/gimbal assembly was given an extensive inspection following the completion of the vibration testing. The interior of the thruster discharge chamber was visually inspected through the ion optics and a small amount of particulate contamination was observed. This was not unexpected, as a significant amount of residue from a mechanical fabrication treatment was observed following the previous engine vibration test,[14] and was difficult to remove entirely during the re-work process. Although thruster pin rotation had been observed in previous testing, most notably in the mass model vibration test, with the additional staking compound applied to the pin in the PM1R testing there was no observable pin rotation in this vibration test program.

Inspection of the bottom of the plasma screen cone revealed a single, relatively large piece of debris. The debris was retrieved from the engine by removing a single section of the plasma screen and appeared to be fibrous material. Analysis of the debris positively identified the material as a match to the fiberglass wire sleeving originally used in the PM1 engine. A small amount of the sleeving material near the harness passthrough on the plasma screen was not removed during the engine re-work and was identified as the likely source.

D. Post-Vibration Gimbal Functional Test

Gimbal functional testing was repeated in the same manner that it had been performed in the pre-vibration characterization. The gimbal was driven to each of the positions shown in Table 5 and the inclination was measured at gimbal thruster bracket A in the radial and tangential directions. All measurements were identical to the pre-vibe measurements of Table 5 with the exception of the tangential inclination in the "Level A, Min B, Max C" step which was 16° in the pre-vibe test and 17° in the post-vibe test. This is within the uncertainty of the measurement and the rounding applied to the data. The total range of the gimbal at this bracket was measured as -19°/+20° in the radial direction and ±17° in the tangential direction, identical to the pre-vibration measurement within uncertainty. The full nineteen-step drive program was then successfully performed to exercise the gimbal motion with the attached thruster. Following completion of the sequence, the pin-puller mockups were re-inserted into the gimbal demonstrating successful and complete return to the stowed and latched position. There was no indication from inspection or test that the gimbal performed any differently after vibration than it did before vibration.

E. Post-Vibration Thruster Functional Test

The post-vibration thruster functional testing was conducted in the same manner as the pre-vibration testing. There were no significant differences in engine performance as compared to the pre-vibration testing. Detailed comparisons of performance data are shown in Section G.

F. Thruster Thermal-Vacuum Test

The first thermal cycle was performed following engine cool down initiated the previous day. The cathode ignition process was initiated approximately seven hours after the reference temperature cooled to the target of -120 °C. The engine started nominally and was brought to full power per the test plan. Heat lamp power was then turned on and the temperature reference location ramped to the 215 °C control temperature in 69 minutes. Thruster operation was held steady at full power (3.52 A, 1800 V) and at the control temperature for 241 minutes before transitioning to the lower power point (3.52 A, 1179 V). After 240 minutes of operation at this condition the thruster was shut down and the cathode heaters immediately turned on for the hot start. The hot start was nominal

and the engine operated in discharge-only mode per the test plan and then at full power before finally turning the engine off. The engine and thermal shroud were allowed to cool for the next thermal cycle. Performance data obtained during the thermal cycles are discussed in a subsequent section.

The second and third thermal cycles were also performed nominally per the test plan. The cathode ignition process was initiated approximately four hours after the reference temperature cooled to the target of -120 °C for the second cycle (four and one half hours for the third cycle). The engine started nominally and was brought to full power per the test plan. Heat lamp power was turned on and the temperature reference location ramped to the 215 °C control temperature in 69 minutes (70 minutes for the third cycle). Thruster operation was held steady at full power and the control temperature for 240 minutes (for both cycles) before transitioning to the lower power. After 242 minutes of operation at this condition (240 minutes for the third cycle) the thruster was shut down and the cathode heaters immediately turned on for the hot start. The hot start was nominal and the engine operated in discharge-only mode per the test plan then at full power before finally turning the engine off (for both cycles). There were no issues with thruster operation during any of the thermal-vacuum testing.

The temperature history for all of the thermal-vacuum testing is shown in Fig. 11. All three gimbal pad temperatures were within a few degrees of each other during the testing, hence only gimbal pad C is shown in the figure for clarity. Note that the coolest of the three gimbal pads was chosen for the control thermocouple. In the hot equilibrium condition, gimbal pad C measured 218 °C.

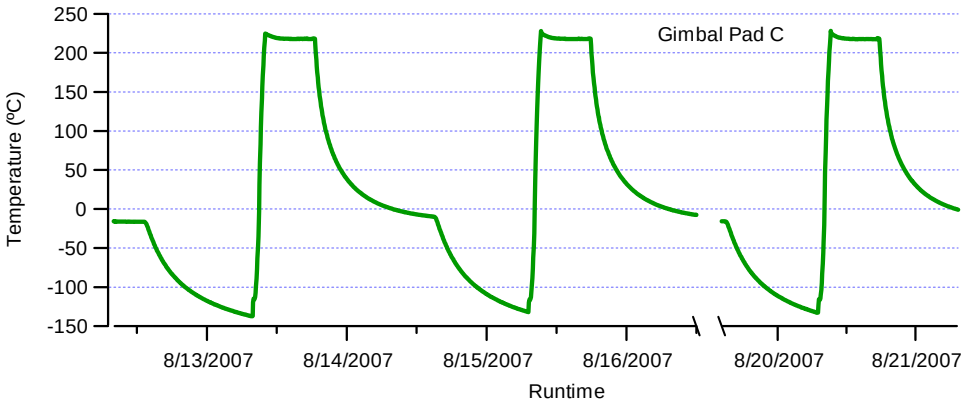

Fig. 11. Thermal Vacuum Testing Temperature Profile.

G. Thruster Functional Testing

Thruster functional testing was performed in the same manner for all functional tests during the environmental test program. Non-controlled and derived engine performance parameters for the lower-power operating conditions are compared for all functional tests in Table 6. It can be seen that there were no major differences in performance throughout the environmental test program at these power levels. Minor differences of up to a few percent were observed in the non-controlled operating parameters, with discharge current variations of several percent at the lowest power. Discharge chamber parameters and accelerator grid current were likely influenced by the tank pressure differences of up to 10% between tests (20% for the first set of tests at the lowest power) caused by graphite panel gas absorption/desorption during the vacuum cycles and rapid tests. Changes in discharge chamber neutral density caused by ingested flow affect discharge performance through the primary electron loss rate and electron temperature, for example.[21] Neutral density near the accelerator grid is also a significant factor in charge-exchange ion production and accelerator grid current. Slight variations in the derived parameters, such as the beam ion energy cost, reflect the differences in measured parameters. The largest effect on the efficiency at the lowest power was the change in discharge power.

Engine performance for the 3.52 A, 1179 V operating condition is shown in Table 7, which includes performance from the three thermal cycles where the engine was operating at elevated temperatures. Again, no major differences in performance were observed with the exception of the accelerator grid current which is almost certainly due to tank pressure variations (it will be shown later that optics performance was essentially unchanged during the testing). Performance data for the full-power operating condition are summarized in Table 8. As for the mid-power cases shown in Table 7, performance was largely the same with the exception of variations in the accelerator grid current due to tank pressure. Note that outgassing from the thruster and/or thermal shroud may have also contributed to the generally-higher measured tank pressures during the thermal cycle testing at elevated temperatures.

Table 6. Engine Performance for the Lower-Power Functional Test Points.

	1.2 A, 679 V			2.0 A, 1179 V		
	Pre-Vibe	**Post-Vibe**	**Post-Thermal**	**Pre-Vibe**	**Post-Vibe**	**Post-Thermal**
Discharge Current (A)	10.4	10.9	10.1	14.2	14.4	14.3
Discharge Voltage (V)	26.1	26.3	26.2	24.2	24.4	24.1
Cathode Keeper Voltage (V)	3.4	3.1	2.9	3.6	3.4	3.0
Accelerator Grid Current (mA)	5.9	4.1	3.9	10.8	8.2	7.5
Neutralizer Keeper Voltage (V)	13.5	13.9	13.8	13.5	13.5	13.4
Power (W)	1130	1140	1120	2750	2760	2750
Tank Pressure (Torr Xe)	2.0E-06	1.5E-06	1.5E-06	2.7E-06	2.4E-06	2.3E-06
Thrust (mN)	49.2	49.2	49.1	108	108	108
Specific Impulse (sec)	2440	2440	2440	3470	3470	3480
Total Efficiency	0.521	0.515	0.524	0.668	0.669	0.672
Beam Ion Energy Cost (eV/ion)	227	238	221	173	176	172

Table 7. Engine Performance for the 3.52 A, 1179 V Operating Condition.

	Pre-Vibe	**Post-Vibe**	**Thermal Cycle #1**	**Thermal Cycle #2**	**Thermal Cycle #3**	**Post-Thermal**
Discharge Current (A)	20.1	20.1	19.7	19.8	19.9	20.2
Discharge Voltage (V)	25.2	25.4	24.9	24.9	25.0	25.0
Cathode Keeper Voltage (V)	5.5	5.5	5.4	5.4	5.4	5.1
Accelerator Grid Current (mA)	24.6	20.4	27.8	24.5	22.4	19.3
Neutralizer Keeper Voltage (V)	11.7	11.7	12.0	11.8	12.1	11.8
Power (W)	4710	4710	4700	4700	4700	4700
Tank Pressure (Torr Xe)	4.8E-06	4.2E-06	4.7E-06	4.4E-06	4.4E-06	4.2E-06
Thrust (mN)	191	191	191	191	191	191
Specific Impulse (sec)	3380	3370	3380	3380	3380	3370
Total Efficiency	0.672	0.672	0.675	0.675	0.675	0.672
Beam Ion Energy Cost (eV/ion)	144	145	139	140	141	144

Table 8. Engine Performance for the 3.52 A, 1800 V Operating Condition.

	Pre-Vibe	**Post-Vibe**	**Thermal Cycle #1**	**Thermal Cycle #2**	**Thermal Cycle #3**	**Post-Thermal**
Discharge Current (A)	18.6	18.6	18.5	18.7	18.8	18.9
Discharge Voltage (V)	24.4	24.4	24.3	24.3	24.4	24.6
Cathode Keeper Voltage (V)	5.5	5.4	5.3	5.2	5.3	5.1
Accelerator Grid Current (mA)	25.9	22.2	29.4	24.1	21.2	18.7
Neutralizer Keeper Voltage (V)	11.8	11.8	12.1	11.8	11.8	11.8
Power (W)	6890	6870	6880	6870	6870	6880
Tank Pressure (Torr Xe)	5.1E-06	4.8E-06	5.2E-06	4.6E-06	4.4E-06	4.3E-06
Thrust (mN)	237	237	237	237	237	237
Specific Impulse (sec)	4180	4180	4180	4180	4180	4180
Total Efficiency	0.705	0.705	0.705	0.706	0.706	0.706
Beam Ion Energy Cost (eV/ion)	129	129	128	129	131	133

Table 9. Ion Optics Functional Test Data.

	Operating Condition	Pre-Vibe	Post-Vibe	Thermal Cycle #1	Thermal Cycle #2	Thermal Cycle #3	Post-Thermal
Perveance Limit (V)	1.2 A, 679 V	570	585	×	×	×	567
	2.0 A, 1179 V	672	696	×	×	×	680
	3.52 A, 1800 V	861	832	×	×	×	837
Electron-Backstreaming Limit (V)	1.2 A, 679 V	-50	-50	×	×	×	-50
	2.0 A, 1179 V	-100	-103	×	×	×	-104
	3.52 A, 1179 V	-122	-122	-129	-124	-126	-120
	3.52 A, 1800 V	-168	-168	-168	-170	-170	-168

Ion optics performance measurements are compared for all functional testing in Table 9. Note that during the thermal vacuum testing perveance measurements were not made, nor were electron backstreaming (EBS) measurements made at the two lower power conditions. There were no measurable changes observed in optics performance as a result of the vibration testing; all the differences were within measurement error and typical data scatter. Differences between pre-vibe and post-vibe perveance limits were in general larger than for the post-vibe and post-thermal measurements. This difference is not significantly larger than the measurement error and typical data scatter, and thus is not necessarily an indication of a hardware change related to the vibration. There was no notable difference in the EBS data acquired throughout the testing.

A significant amount of beam current density data were acquired during the environmental testing. Shown in Fig. 12 are data acquired during two functional test operating conditions at the standard 45 mm distance from the ion optics face. It can be seen from the data that there is essentially no difference in the beam profiles recorded before and after the vibration and thermal tests.

Results of the neutralizer characterization for all functional tests are shown in Fig. 13. The spot-to-plume-mode transition, as defined by the presence of 5 V peak-to-peak fluctuations in the neutralizer keeper voltage, was at 3.3 sccm for the pre-vibe and post-thermal tests and at 3.4 sccm for the post-vibe test. The difference in this result is not considered to be significant.

Cathode ignition times were recorded for all engine starts during the environmental test program and are reported in Table 9. Cathode ignition time is defined as the time elapsed from the beginning of the ignition procedure until a full-level plasma discharge is produced. Starts are labeled ambient if the engine and cathode were at ambient chamber temperatures prior to the start attempt; cold starts were those performed after cooling of the engine with the thermal shroud at liquid nitrogen temperatures; warm starts were those performed within approximately one hour after previous cathode operation; and hot restarts were those performed within minutes after previous cathode operation. Neutralizer ignition times showed a slight dependence on cathode temperature during the environmental testing. The average ignition

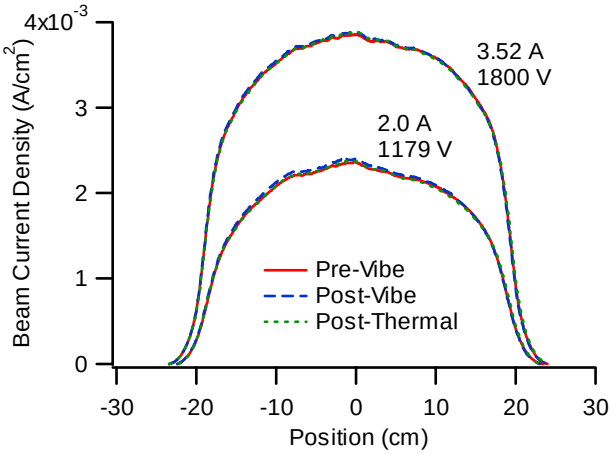

Fig. 12. Pre- and Post-Vibration Beam Current Density Measured 45 mm from Accelerator Grid.

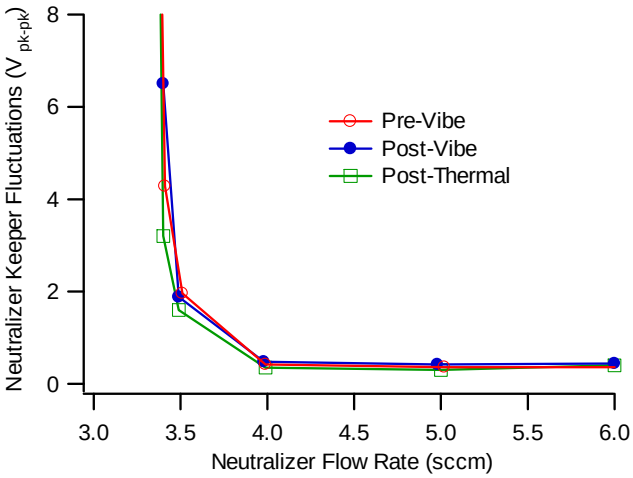

Fig. 13. Neutralizer Characterization Test Results.

time for a warm/hot neutralizer was 3.5 minutes, and for an ambient/cold neutralizer was 4.0 minutes. The discharge cathode ignition time showed a stronger dependence on temperature. The average ignition time for warm/hot cathodes was 3.9 minutes, whereas the ambient/cold start times averaged 5.2 minutes. There did not appear to be any effect on ignition time due to the vibration or thermal-vacuum tests from the limited data available. Due to the longer discharge cathode ignition times and appreciable scatter in this and the previously reported testing,[14] discharge cathode ignition time findings will require further analysis with regard to life validation and system-level impact.

Table 9. Cathode Ignition Times.

Test	Discharge Cathode Ignition Time (min)	Neutralizer Ignition Time (min)	Notes
Pre-Vibe Performance	4.6	3.6	Warm start
	6.0	5.0	Ambient start
Post-Vibe Performance	4.9	3.6	Warm start
	3.5	3.5	Hot restart
	5.1	4.2	Ambient start
Thermal Cycle #1	5.9	4.2	Cold start
	3.5	3.5	Hot restart
Thermal Cycle #2	4.5	3.5	Cold start
	3.5	3.5	Hot restart
Thermal Cycle #3	6.1	3.7	Cold start
	3.5	3.5	Hot restart
Post-Thermal Performance	3.8	3.6	Ambient start

H. Final Inspection

After completion of the post-thermal functional testing the engine was removed from the vacuum facility and given a complete physical and electrical inspection. There were no significant findings as a part of these inspections.

IV. Conclusion

Environmental testing of the NEXT PM1R ion engine and gimbal assembly was completed according to NEXT project requirements, and both were found to be well-designed against environmental requirements based on the results reported herein.

Random vibration testing was performed and successfully completed at levels of 10.0 G_{rms} in three axes at two minutes per axis for the PM1R thruster and breadboard gimbal assembly. Although contamination was observed inside the thruster after completion of vibration testing, it was linked to sources identified prior to this test program that could not be completely removed in this hardware. Engineering solutions are available and contamination is not expected to be an issue in a flight-model hardware design. Pre- and post-test sine surveys showed some significant differences indicating some changes to the test hardware, likely a slight hardware settling at the thruster capture interface. Similar types of sine shifts were observed in vibration testing with this gimbal and with the PM1 engine and a thruster mass model, and are presently under investigation. Gimbal functional tests performed prior to and after the vibration test were successful with nearly identical performance in each instance.

The thruster was successfully subjected to three thermal cycles of temperature range -120 °C to 215 °C. There were no issues found with thruster startup at cold temperatures, operation during rapid temperature rates of increase, operation at hot temperatures, or hot thruster restarts.

Functional tests of the engine and the gimbal were performed prior to and after both vibration and thermal vacuum testing, and thruster performance was observed to be nominal throughout the test program. There were noticeable changes in some thruster operational parameters, likely related to modest differences in tank pressure between different test phases, but no indication of a major change in thruster performance or operation resulting from exposure to the vibration and thermal environments. Similarly, there was no major change in ion optics performance or beam current density data. Although neutralizer cathode ignition times were consistent and showed little dependence on temperature, the discharge cathode ignition times showed greater scatter and a stronger dependence on temperature.

No new findings were generated as a result of the reworked PM1R environmental testing. Most of the findings of the previous PM1 engine testing were successfully resolved, e.g. cathode heater termination structural integrity and loose fasteners. The remaining issues, e.g. contamination, appear to have straightforward engineering solutions and should be resolved without difficulty prior to a hardware qualification program.

Acknowledgments

The work described in this paper was carried out by the Jet Propulsion Laboratory, California Institute of Technology, under a contract with the National Aeronautics and Space Administration. The PM1R Environmental Test program, funded by NASA's In-Space Propulsion Technology Program, was successfully accomplished through the efforts of a multi-organizational team. The work was performed under the NEXT Project, led by the NASA Glenn Research Center, with Scott Benson as the Project Manager and Mike Patterson as the Principal Investigator. Allison Owens and Ray Swindlehurst of the JPL Electric Propulsion Group were responsible for designing, configuring, and operating the test facility. Rich Ebner, Tim Werner, and Doug Perry of the JPL Environmental Test Lab were responsible for setup, instrumentation, and performing the vibration test. Their efforts and contributions are greatly appreciated.

References

1. M.J. Patterson and S.W. Benson, "NEXT Ion Propulsion System Development Status and Performance," AIAA Paper 2007-5199, 43rd Joint Propulsion Conference, Cincinnati, OH, July 2007.
2. D. Oh, S. Benson, K. Witzberger, and M. Cupples, "Deep Space Mission Applications for NEXT: NASA's Evolutionary Xenon Thruster," AIAA 2004-3806, 40th Joint Propulsion Conference, Fort Lauderdale, FL, July 2004.
3. J.R. Brophy, "NASA's Deep Space 1 Ion Engine," Review of Scientific Instruments, Vol. 73, No. 2, Feb. 2002, pps. 1071-1078.
4. J.R. Brophy, et. al, "Development and Testing of the Dawn Ion Propulsion System," AIAA 2006-4319, 42nd Joint Propulsion Conference, Sacramento, CA, July 2006.
5. G.C. Soulas, M.T. Domonkos, and M.J. Patterson, "Performance Evaluation of the NEXT Ion Engine," AIAA 2003-5278, 39th Joint Propulsion Conference, Huntsville, AL, July 2003.
6. G.C. Soulas, H. Kamhawi, M.J. Patterson, M.A. Britton, and M.M. Frandina, "NEXT Ion Engine 2000 Hour Wear Test Results," AIAA 2004-3791, 40th Joint Propulsion Conference, Fort Lauderdale, FL, July 2004.
7. M.J. Patterson, L.R. Piñero, R. Aadland, and D. Komm, "NEXT Ion Propulsion System: Single-String Integration Test Results," JANNAF Conference, May 2004.
8. D.A. Herman, G.C. Soulas, and M.J. Patterson, "NEXT Long-Duration Test after 11,570 h and 237 kg of Xenon Processed," IEPC-2007-033, to be presented at the 30th International Electric Propulsion Conference, Florence, Italy, Sept. 17-20, 2007.
9. M.J. Patterson, J. Foster, H. McEwen, E. Pencil, J. Van Noord, and D. Herman, "NEXT Multi-Thruster Array Test – Engineering Demonstration," AIAA 2006-5180, 42nd Joint Propulsion Conference, Sacramento, CA, July 2006.
10. W.A. Hoskins, F.C. Wilson, J. Polaha, L. Talerico, M.J. Patterson, G.C. Soulas, and J. Sovey, "Development of a Prototype Model Ion Thruster for the NEXT System," AIAA 2004-4111, 40th Joint Propulsion Conference, Fort Lauderdale, FL, July 2004.
11. D.A. Herman, G.C. Soulas, and M.J. Patterson, "Performance Evaluation of the Prototype-Model NEXT Ion Thruster," AIAA 2007-5212, 43rd Joint Propulsion Conference, Cincinnati, OH, July 2007.

12. J.R. Anderson, J.S. Snyder, J. Van Noord, and G.C. Soulas, "Thermal Development Test of the NEXT PM1 Ion Engine," AIAA 2007-5217, 43rd Joint Propulsion Conference, Cincinnati, OH, July 2007.
13. J.L. Van Noord, "NEXT Ion Thruster Thermal Model," AIAA 2007-5218, 43rd Joint Propulsion Conference, Cincinnati, OH, July 2007.
14. J.S. Snyder, J.R. Anderson, J. Van Noord, and G.C. Soulas, "Environmental Testing of the NEXT PM1 Ion Engine," AIAA 2007-5275, 43rd Joint Propulsion Conference, Cincinnati, OH, July 2007.
15. W.A. Hoskins, R.S. Aadland, N.J. Meckel, L.A. Talerico, and J.M. Monheiser, "NEXT Ion Propulsion System Production Readiness," AIAA 2007-5856, 43rd Joint Propulsion Conference, Cincinnati, OH, July 2007.
16. D.A. Vaughan, "Gimbal Development for the NEXT Ion Propulsion System," AIAA 2005-3865, 41st Joint Propulsion Conference, Tucson, AZ, July 2005.
17. J.S. Snyder, M.R. O'Connell, J.P. Fernandez, G.Wang, R.S. McNabb, Jr., and D. Crumb, "Vibration Test of a Breadboard Gimbal for the NEXT Ion Engine, AIAA 2006-4665, 42nd Joint Propulsion Conference, Sacramento, CA, July 2006.
18. NASA-HDBK-7004B, "Force Limited Vibration Testing," NASA Technical Handbook, January 31, 2003.
19. S.W. Benson, M.J. Patterson, D.A. Vaughan, A.C. Wilson, and B.R. Wong, "NASA's Evolutionary Xenon Thruster (NEXT) Phase 2 Development Status," AIAA 2005-4070, 41st Joint Propulsion Conference, Tucson, AZ, July 2005.
20. J.A. Christensen, et. al, "Design and Fabrication of a Flight Model 2.3 kW Ion Thruster for the Deep Space 1 Mission," AIAA 98-3327, 34th Joint Propulsion Conference, Cleveland, OH, July 1998.
21. D.M. Goebel, R.E. Wirz, and I. Katz, "Analytical Ion Thruster Discharge Performance Model, AIAA 2006-4486, 42nd Joint Propulsion Conference, Sacramento, CA, July 2006.